J|A|C|S
ARTICLES
Published on Web 09/21/2006

Organic−Organic Epitaxy of Incommensurate Systems: Quaterthiophene on Potassium Hydrogen Phthalate Single Crystals

Marcello Campione,*,† Adele Sassella,† Massimo Moret,† Antonio Papagni,† Silvia Trabattoni,† Roland Resel,‡ Ondrej Lengyel,‡ Valentina Marcon,§ and Guido Raos§

Contribution from the Department of Materials Science, University of Milan "Bicocca", Via R. Cozzi 53, I-20126, Milano, Italy, Institute of Solid State Physics, Graz University of Technology, Petersgasse 16, A-8010 Graz, Austria, and Department of Chemistry, Materials and Chemical Engineering "Giulio Natta", Politecnico di Milano, Via Mancinelli 7, I-20131 Milano, Italy

Received December 27, 2005; Revised Manuscript Received August 16, 2006; E-mail: marcello.campione@mater.unimib.it

Abstract: Hot-wall epitaxy and molecular-beam epitaxy have been employed for growing quaterthiophene thin films on the (010) cleavage face of potassium hydrogen phthalate, and the results are compared in terms of film properties and growth mode. Even if there is no geometrical match between substrate and overlayer lattices, these films are epitaxially oriented. To investigate the physical rationale for this strong orientation effect, optical microscopy, atomic force microscopy, and X-ray diffraction are employed. A clear correlation between the morphology of the thin films and the crystallographic orientation is found. The results are also validated by surface potential calculations, which demonstrate the primary role played by the corrugation of the substrate surface.

1. Introduction

A large part of fundamental and applied research on organic materials is devoted to the study of the mechanisms leading to molecular aggregation.[1] Applications to fields as disparate as organic electronics and pharmaceuticals depend on the self-organizing properties of molecular systems, which rely in turn on a subtle balance of weak intermolecular forces. Different crystal polymorphs can have rather different electron mobilities or solubilities, to mention two important properties for electronic and pharmaceutical applications. Therefore, the ability to control crystal nucleation and growth represents both a challenge and an opportunity. These nonequilibrium phenomena provide an alternative and more flexible route for obtaining new crystalline polymorphs or well-ordered thin films than the thermodynamic one. Indeed, the knowledge of these nonequilibrium mechanisms allows researchers to control the growth of the materials, with the aim to tune their structure and morphology and ultimately their physical properties. In this way, methods to enhance the performance of devices based on organic active layers can also be developed. Finally, it is interesting to observe that the complexity of molecular shapes and the advances in synthetic chemistry allow a far more complex and appealing variety of crystalline structures and morphologies than in inorganic materials, being in addition the starting point for the development of new models and theories.[2]

The study of the aggregation mechanism of materials has to focus on the investigation of solid samples at the early stage of their growth, i.e., on thin solid films. Recently, sophisticated vapor-phase techniques, well-established in the field of inorganic semiconductors, have been successfully applied in the growth of high-quality thin films of molecular organic materials.[3] Among these techniques, molecular-beam epitaxy (MBE) and hot-wall epitaxy (HWE) are the ones offering the best compromise between adaptability to the requirements of organics and high control in the growth process.[4] MBE is a cold-wall method which allows the growth of high-quality layers at a low rate and usually under far-from-equilibrium conditions. On the other hand, HWE permits high growth rates and a crystallization occurring under near-equilibrium conditions. Hence, substantial differences in the thermodynamics and kinetics of growth characterize these two techniques.

The possibility to grow oriented and highly crystalline thin films relies on the choice of a suitable substrate, together with the right choice of source and substrate temperature and residual pressure in the growth chamber. The orientation effect of the substrate is translated according to the registry between substrate and overlayer lattices. While for inorganics epitaxial growth is

† University of Milan "Bicocca".
‡ Graz University of Technology.
§ Politecnico di Milano.

(1) Witte, G.; Wöll, C. *J. Mater. Res.* **2004**, *19*, 1889.
(2) (a) Agranovich, V. M.; Bassani, F. *Electronic Excitations in Organic Based Nanostructures*; Academic Press: Orlando, 2003. (b) Lehn, J.-M. *Supramolecular Chemistry: Concepts and Perspectives*; VCH: Weinheim, 1995. (c) Desiraju, G. R. *Crystal Design: Structure and Function*; John Wiley and Sons: Chichester, 2003. (d) Gavezzotti, A. *Modell. Simul. Mater. Sci. Eng.* **2002**, *10*, R1. (e) Dunitz, J. D. *Chem. Commun.* **2003**, 545. (f) Piana, S.; Reyhani, M.; Gale, J. D. *Nature* **2005**, *483*, 70.
(3) Forrest, S. R. *Chem. Rev.* **1997**, *97*, 1793.
(4) (a) Stifter, D.; Sitter, H. *Appl. Phys. Lett.* **1995**, *66*, 679. (b) Lopez-Otero, A. *Thin Solid Films* **1978**, *49*, 3.

10.1021/ja058771w CCC: $33.50

possible only when lattice mismatch falls within a few percent,[5] for organics the onset of this phenomenon requires far less restrictive conditions. In the case of organic overlayers grown on inorganic substrates, many examples reported in the literature demonstrate that, even when the lattice mismatch is of the order of several tens of percent, an orientation effect may be accomplished through a more relaxed epitaxial condition, the so-called *coincident epitaxy*.[6] Under this condition, only a subgroup of lattice points of the overlayer and substrate are in perfect registry, and this is usually achieved for one or more particular azimuthal orientations of the two lattices.

The technological drive toward "all-organic" electronics provides a strong motivation for exploring the possibility of growing organic semiconductor films on polymeric or molecular substrates. In this case, the large size and low symmetry of the unit cells of the substrate and of the overlayer may easily determine a condition of complete incommensurism. This means that no particular azimuthal orientation of the overlayer crystal lattice can provide some coincidence between thin-film and substrate lattice points. At first, this might seem to prevent the possibility of obtaining well-ordered films—a desirable features for several applications. Nonetheless, some examples of organic–organic epitaxy show that a strong orientation effect can be accomplished also under a condition of complete incommensurism.[7] This behavior was observed, for example, in thin films of diacetylene derivatives deposited on the (010) surface of potassium hydrogen phthalate (KAP)[7a] and tentatively explained as *molecular epitaxy*, where the orientation effect is believed to be driven by a favorable insertion of molecular moieties between KAP phenyl rings. A similar orientational behavior was recently observed in quaterthiophene (4T) thin films grown on KAP(010) by MBE,[8] where the bulk structures of the film and substrate are incommensurate. However, the molecular and single-crystal structures of 4T (see Figure 1) hinder the occurrence of any possible insertion of molecular moieties between the prominent substrate phenyl rings.

In this work, 4T overlayers are grown under controlled conditions on KAP(010) by MBE and HWE; these films were characterized by optical microscopy (OM), atomic force microscopy (AFM), and X-ray diffraction (XRD), which provide a detailed analysis of the differences in film morphology, structure, and orientation of crystalline domains in relation to the different growth conditions of the two techniques. In this way, new insights into the mechanism governing the epitaxy of incommensurate systems are obtained, demonstrating that it is the surface morphology (or "corrugation") of the substrate that is primarily responsible for driving the film orientation, rather than simply its crystalline periodicity or the possibility to form molecular complexes. This conclusion is further validated by the theoretical prediction of a potential energy minimum for the 4T/KAP interface with the observed orientations, demonstrating that the orientation effect does not occur solely for a single adsorbed molecule but corresponds to the achievement of a stable configuration of the bulk system.

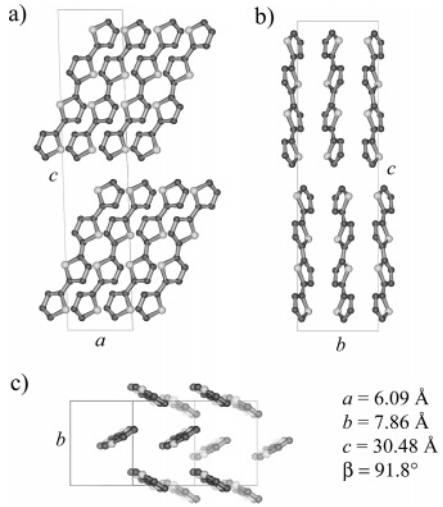

Figure 1. Crystal structure of the α4T/LT polymorph as viewed along the (a) [010], (b) [100], and (c) [201] directions. Hydrogen atoms are omitted.

2. Methods

2.1. 4T Synthesis. To synthesize 4T ($C_{16}H_{10}S_4$) in significant amount (hundreds of milligrams scale) and of suitable purity without resorting to long and tedious purification,[9] we have considered a procedure[10] based on coupling of two bithiophene units, catalyzed by Pd^{2+}, in a mixture of CH_3CN, MeOH, and H_2O as solvents (see Scheme 1).

Scheme 1. Homocoupling Reaction Catalyzed by Pd^{2+}

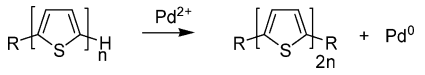

Two different ways to regenerate Pd^{2+} from Pd^0 are reported,[10] namely bubbling air in the reaction mixture or using benzoquinone. To improve the reported chemical yields, we looked for a more efficient oxidant agent. The coupling reaction was performed using several different oxidant agents: (i) $CuCl_2$, which is the well-known reoxidant agent of Pd^0 in the Wacker process;[11] (ii) Ag^+ salts; and (iii) 7,7′,8,8′-tetracyanoquinodimethane (TCNQ). Yields up to 45% were obtained with CF_3COOAg, while only a modest 26% was obtained with $CuCl_2$. With TCNQ, the complex between 4T and TCNQ was collected in 30% yield. The formation of charge-transfer complexes between oligothiophenes and TCNQ is well documented in the literature.[12] Surprisingly, when AgF was used, the yield of 4T dropped to 23%. In a recent work by Masui et al., where different Ag^+ salts were used in homocoupling of thiophene derivatives, it was underlined that the production of HF as a byproduct of the coupling process has a detrimental effect on the yield of bithiophenes.[13] The authors proposed the use of dimethyl sulfoxide (DMSO) to trap HF as a way to limit its negative effect. Applying this experimental condition to the synthesis of 4T considerably helped to improve the yields. For example, the yield increased to 42% with 0.18 equiv of Pd^{2+} and further increased to 76% when 0.04 equiv of Pd^{2+} was used. This latter condition was also applied to the synthesis of α,ω-dihexylquaterthiophene (α,ω-DH4T), which was collected in 86% yield. The results are summarized in Table 1.

(5) Herman, M. A.; Sitter, H. *Molecular Beam Epitaxy*; Springer-Verlag: Berlin and Heidelberg, 1989.
(6) (a) Hooks, D. E.; Fritz, T.; Ward, M. D. *Adv. Mater.* **2001**, *13*, 227. (b) Koma, A. *Prog. Crystal Growth Charact.* **1995**, *30*, 129. (c) Mannsfeld, S. C. B.; Fritz, T. *Phys. Rev. B* **2005**, *71*, 235405.
(7) (a) Le Moigne, J.; Kajzar, F.; Thierry, A. *Macromolecules* **1991**, *24*, 2622. (b) Da Costa, V.; Le Moigne, J.; Oswald, L.; Pham, T. A.; Thierry, A. *Macromolecules* **1998**, *31*, 1635. (c) Mitchell, C. A.; Yu, L.; Ward, M. D. *J. Am. Chem. Soc.* **2001**, *123*, 10830.
(8) (a) Sassella, A.; Besana, D.; Borghesi, A.; Campione, M.; Tavazzi, S.; Lotz, B.; Thierry, A. *Synth. Met.* **2003**, *138*, 125. (b) Timpanaro, S.; Sassella, A.; Borghesi, A.; Porzio, W.; Fontane, P.; Goldmann, M. *Adv. Mater.* **2001**, *13*, 127.
(9) Trabattoni, S.; Laera, S.; Mena, R.; Papagni, A.; Sassella, A. *J. Mater. Chem.* **2004**, *14*, 171.
(10) Hanson, E. L.; Schwartz, J.; Nickel, B.; Koch, R.; Danisman, M. F. *J. Am. Chem. Soc.* **2003**, *125*, 16074.
(11) Parrish, J. P.; Flanders, V. L.; Floyd, R. J.; Jung, K. W. *Tetrahedron Lett.* **2001**, *42*, 7729.
(12) Hotta, S.; Waragai, K. *Synth. Met.* **1989**, *32*, 395.
(13) Masui, K.; Ikegami, H.; Mori, A. *J. Am. Chem. Soc.* **2004**, *126*, 5074.

Table 1. Homocoupling Reaction of 2T

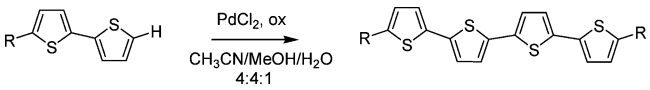

R	$PdCl_2$ (equiv)	oxidant reagent	solvent	reaction time (h)	yield (%)
H (**a**)	0.18	air	CH_3CN, MeOH, H_2O	50	36
H (**b**)	0.18	$CuCl_2$ (1 equiv)/air	CH_3CN, MeOH, H_2O	50	26
H (**c**)	0.18	TCNQ (0.18 equiv)/air	CH_3CN, MeOH, H_2O	50	—[a]
H (**d**)	0.18	CF_3COOAg (1 equiv)	CH_3CN, MeOH, H_2O	22	45
H (**e**)	0.01	CF_3COOAg (1 equiv)	CH_3CN, MeOH, H_2O	80	–
H (**f**)	0.18	AgF (2 equiv)	CH_3CN, MeOH, H_2O	90	23
H (**g**)	0.18	AgF (2 equiv)	DMSO (35 °C)	6	42
H (**h**)	0.04	AgF (2 equiv)	DMSO (35 °C)	34	76
C_6H_{13}	0.04	AgF (2 equiv)	DMSO (35 °C)	8	86
C_6F_{13}	0.03	AgF (2 equiv)	DMSO (35 °C)	36	–

[a] The charge-transfer complex between 4T and TCNQ was collected in 30% yield.

The procedure fails in the synthesis of perfluoro-α,ω-DH4T, probably due to the deactivation effect of perfluorinated alkyl chains. The basic synthesis method was also effective in obtaining sexithiophene from terthiophene, but with a poor yield, probably due to a lack of reactivity of oligothiophenes in the coupling reaction when the number of thiophene units increases.

2.2. Thin Film Deposition. KAP single crystals were purchased from Ekspla (Vilnius, Lithuania). The KAP crystal structure belongs to the orthorhombic system (space group $Pca2_1$), with cell parameters $a = 9.61$ Å, $b = 13.33$ Å, and $c = 6.48$ Å.[14] The molecularly flat (010) surface of the crystal is prepared by mechanical cleavage in air immediately before the substrate is introduced in the growth chamber, with cleaving direction approximately parallel to $[101]_{KAP}$.[15] The cleavage surface is a corrugated surface consisting exclusively of phenyl rings tilted relative to each other; the potassium ions are located in layers beneath.

Two polymorphs of bulk 4T are known: α4T/LT and α4T/HT, both of which are classified as having layered herringbone structure.[2c] A sketch of the structure of the α4T/LT polymorph is depicted in Figure 1. α4T/LT and α4T/HT belong to the same monoclinic system (space group $P2_1/c$, with four molecules per unit cell, and $P2_1/a$, with two molecules per unit cell, respectively), with lattice parameters $a = 6.09$ Å, $b = 7.86$ Å, $c = 30.48$ Å, $\beta = 91.80°$, and $a = 8.94$ Å, $b = 5.75$ Å, $c = 14.34$ Å, $\beta = 97.22°$, respectively.[16] The main difference between the structures is the tilt angle of the long molecular axis within the herringbone layers. The thin films were grown in ultra-high-vacuum (UHV) conditions by organic MBE and in high vacuum by HWE. MBE samples were deposited at a base pressure below 5×10^{-10} Torr, with 160 °C as source temperature for 4T, keeping the substrate at room temperature. The source was a Knudsen-type effusion cell with double heater and double temperature control;[17] a quartz microbalance installed close to the substrate was used to dose the material.[18] A deposition rate of about 0.5 nm min^{-1} was maintained to grow all the films. HWE samples were deposited under 10^{-6} Torr pressure at a source temperature of 135 °C, wall temperature 120 °C, keeping the substrate at 25 °C, with a deposition time of 10 min. The thicknesses of the samples investigated here are of the order of tens of nanometers.

The optical micrographs of the samples were collected using a Leica DMLM microscope in reflection mode with differential interference contrast.

2.3. Atomic Force Microscopy. AFM measurements were carried out in air or dry nitrogen atmosphere using a Digital Instrument Nanoscope IIIa MMAFM equipped with E- and J-type scanners. Images were collected in tapping mode, with single-beam silicon cantilevers with typical force constant of 40 N/m and resonance frequency of 300 kHz. Scanner-induced artifacts in the collected images were corrected by means of a polynomial fit procedure of order up to three.

2.4. X-ray Diffraction. Specular scans ($\theta/2\theta$ mode) are performed with a conventional powder diffractometer in Bragg–Brentano parafocusing geometry, using Cu Kα radiation and a secondary graphite monochromator. A Philips X'Pert system with an ATC3 texture cradle was employed for pole-figure (PF) measurements performed in Schultz reflection geometry using Cr Kα radiation and a secondary graphite monochromator. The software packages POWDER CELL[19] and STEREOPOLE[20] were used for XRD data analysis. The measurements were performed by ψ-steps of 2°, φ-steps of 5°, and 20 s measurement time for each ψ/φ pair. Some intensity of the KAP substrate is observed in the 4T pole figures. These intensities are undoubtedly attributable to scattering of higher harmonics of Cr Kα radiation on KAP planes.

2.5. Theoretical Calculations. The orientational effect of KAP on 4T was also investigated by computer simulation. Specifically, the preferential orientation of two LT-like monolayers of 4T on KAP(010) was determined by energy minimization, using the TINKER 4.1 molecular modeling package.[21] Our force field for 4T[22] is based on the MM3 parametrization for the intramolecular terms,[23] supplemented with an accurate torsion potential[24] and atomic point charges from high-level ab initio calculations. Lennard-Jones parameters were borrowed from OPLS-AA.[25] In our experience, these nonbonded parameters are superior to those of MM3 which were used in a previous study,[26] since they predict oligothiophene crystal cell parameters and heats of sublimation in better agreement with experiment.[22] Similar criteria were used in the construction of our force field for KAP, which is mainly based on OPLS-AA.

3. Results

3.1. Morphology and Structure. Two representative optical images of the surface of the films grown by HWE and MBE are reported in Figure 2a and b, respectively. These images show the presence of oriented white segments and a uniform gray background. The white segments represent needle-like crystallites, and their bright contrast is probably due to light diffusion. The uniform background can be assigned to a flat film phase or to the bare substrate surface.

From the optical micrographs, the substantial difference between HWE and MBE films resides in the density of the needle-like crystallites, which is far lower when MBE conditions are employed. Nonetheless, the size and orientation of these needles are similar for the two growth techniques: they display a length of about 10 μm and are oriented at angles of ±63° and ±5° to c_{KAP} (within an uncertainty of ±2°).[8a]

Further details of the morphology of MBE films are obtained by AFM measurements. Figure 3a reports an AFM image collected on a 10 nm thick film, where oriented needles at their

(14) Eremina, T. A.; Furmanova, N. G.; Malakhova, L. F.; Okhrimenko, T. M.; Kuznetsov, V. A. *Crystallogr. Rep.* **1993**, *38*, 554.
(15) Borc, J.; Sangwal, K. *Surf. Sci.* **2004**, *555*, 1.
(16) Siegrist, T.; Kloc, C.; Laudise, R. A.; Katz, H. E.; Haddon, R. C. *Adv. Mater.* **1998**, *10*, 379.
(17) Tubino, R.; Borghesi, A.; Dalla Bella, L.; Destri, S.; Porzio, W.; Sassella, A. *Opt. Mater.* **1998**, *9*, 437.
(18) Campione, M.; Cartotti, M.; Pinotti, E.; Sassella, A.; Borghesi, A. *J. Vac. Sci. Technol. A* **2004**, *22*, 482.
(19) Kraus, W.; Nolze, G. *J. Appl. Crystallogr.* **1996**, *29*, 301.
(20) Salzmann, I.; Resel, R. *J. Appl. Crystallogr.* **2004**, *37*, 1029.
(21) (a) Ponder, J. W. *TINKER: Software Tools for Molecular Design*, 4.1 ed.; Washington University School of Medicine: Saint Louis, MO, 2003. (b) Ren, P.; Ponder, J. W. *J. Comput. Chem.* **2002**, *23*, 1497. (c) Ren, P.; Ponder, J. W. *J. Phys. Chem. B* **2003**, *107*, 5933.
(22) Marcon, V.; Raos, G. *J. Phys. Chem. B* **2004**, *108*, 18053.
(23) (a) Allinger, N. L.; Yuh, Y. H.; Li, J.-H. *J. Am. Chem. Soc.* **1989**, *111*, 8551. (b) Li, J.-H.; Allinger, N. L. *J. Am. Chem. Soc.* **1989**, *111*, 8566 and 8576.
(24) Raos, G.; Famulari, A.; Marcon, V. *Chem. Phys. Lett.* **2003**, *379*, 364.
(25) Jorgensen, W. L.; Maxwell, D. S.; Tirado-Rives, J. *J. Am. Chem. Soc.* **1996**, *118*, 11225.
(26) Marcon, V.; Raos, G. *J. Am. Chem. Soc.* **2006**, *128*, 1408.

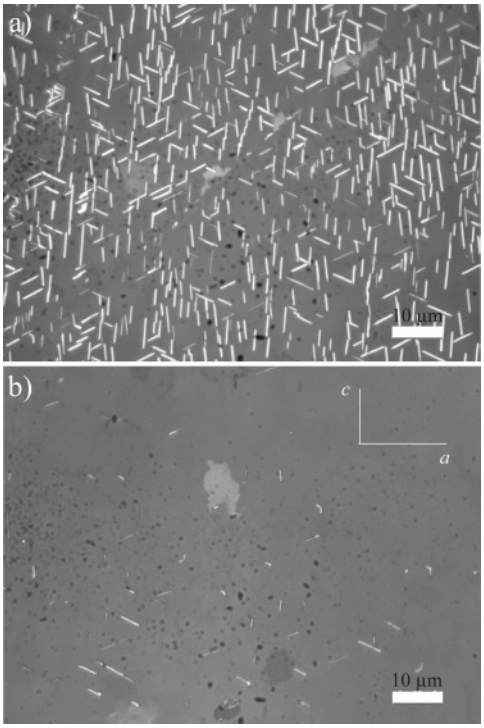

Figure 2. Optical micrographs of the 4T films grown on KAP(010) by (a) HWE and (b) MBE. Bright segments represent needle-like crystallites. The orientation of the substrate surface lattice reported on the top-right of panel b applies to both images.

early stage of growth (with a length of about 1 μm) are observed, together with a uniform flat phase covering about the 50% of the substrate surface. For thicker films, up to 80 nm, monomolecular terraces are clearly visible on the surface of the flat phase, belonging to growth hillocks originating from screw dislocations, visible in Figure 3b. Longer needles are also present on the surface; the needle width in both images in Figure 3 is the upper limit, being affected by the AFM tip shape and dimension.

A structural characterization of 4T thin films grown on KAP(010) by MBE was performed by transmission electron microscopy.[8a] Evidence of the presence of crystallites of the low-temperature polymorph (α4T/LT[16]) oriented with different contact planes was found. Molecules in the islands are standing almost upright relative to the substrate plane, whereas the molecular axes are more tilted toward the substrate in the case of needles. The structural properties of 4T films grown on KAP by the two techniques are investigated by XRD. Figure 4 shows the patterns of the bare KAP substrate, a 4T film grown by MBE, and a 4T film grown by HWE. In the latter, diffraction peaks are indexed in accordance with the crystal structure of the α4T/LT polymorph:[16] reflections of the 00*l* planes are revealed, with the systematic extinction of the odd-*l* planes, in agreement with the symmetry of the system considered, and a reflection of the (020) planes is also visible. Excepting this latter reflection, all the aforementioned reflections are present in the MBE films as well. Additionally, the diffraction patterns collected on these films report two peaks at $2\theta = 22.21°$ and 35.50°, respectively (arrows in Figure 4), which cannot be considered as coming from crystallographic planes of neither the α4T/LT nor the α4T/HT polymorphs.

The presence of the 00*l* and 020 reflections indicate crystalline domains contacting the substrate with the *ab* and *ac* planes,

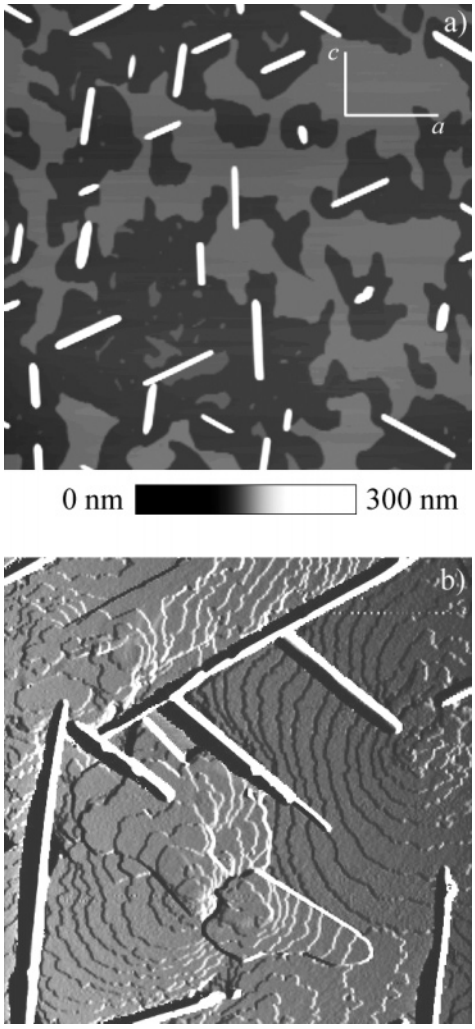

Figure 3. 10×10 μm^2 AFM images of the surface of (a) a 10 nm thick 4T film (height image) and (b) an 80 nm thick 4T film (error signal) grown on KAP(010) by MBE. The orientation of the substrate surface lattice for both images is reported on the top-right of panel a.

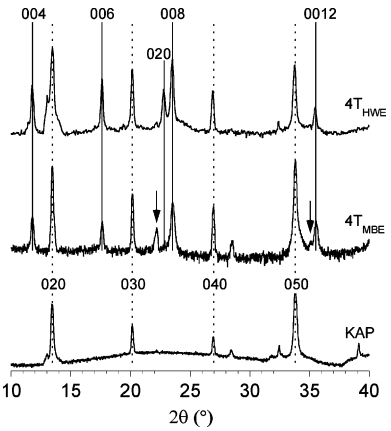

Figure 4. $\theta/2\theta$ specular scans collected on the bare KAP substrate and on 4T thin films grown by HWE and MBE on KAP(010). Dashed and solid lines distinguish reflections of the substrate (indexed in the lower panel) and the α4T/LT phase (indexed in the upper panel), respectively. Arrows indicate reflections which cannot be indexed with neither the α4T/LT nor the α4T/HT structures.

respectively; in the first case, the long axes of molecules form an angle of 24.8° to the substrate plane normal, whereas in the latter the molecular axes are parallel to the substrate surface

and molecules lie edge-on, with the least-squares plane of the quaterthiophene moiety tilted by 31.6° (half the herringbone angle) to the substrate plane.

The observed morphologies of 4T on KAP are typical for thin films of herringbone-type crystals.[27] The terrace-like morphology consists of molecules with end-on orientation, which is, in the present case, the crystallographic (001) plane parallel to the substrate surface. Needle-like morphology arises due to molecules which are aligned with their long molecular axes parallel to the surface of the substrate (edge-on or flat-on): in the present case, the (010) plane of α4T/LT is parallel to the KAP(010) surface.

Rocking curves (not shown) were preliminarily collected on the samples to determine their mosaicity. Typical values for fwhm for the $(030)_{KAP}$, $(020)_{4T}$, and $(008)_{4T}$ reflections are 0.75°, 0.83°, and 0.79°, respectively. The rocking curves are measured with low experimental resolution; however, the only slightly larger values for the fwhm of the 4T diffraction peaks (in comparison with those of the single-crystal KAP) reveal the highly preferred orientation of the 4T crystallites within the films.

3.2. Film Texture. The crystal structure and the out-of-plane orientation of the 4T crystallites were identified by XRD specular scans. The texture analysis was performed to determine the in-plane orientation and order of the 4T crystallites relative to the KAP surface, in other words, the epitaxial relationships between the thin film and the substrate.

An established strategy for predicting epitaxial relationships involves the calculation of the lattice mismatch as a function of the in-plane (azimuthal) orientation. We report in Figure 5 the results of this analysis performed with the program EpiCalc[28] for the orientations found experimentally for 4T on KAP(010). This approach consists of a real-space analytical expression that analyzes the phase coherence between overlayer and substrate lattices at a specific azimuthal angle for a specific set of lattice parameters. The surface potentials of overlayer and substrate are described as simple plane waves so that the output of the analytical function can be a dimensionless potential V/V_0 at specific angles. The functions return discrete values of $V/V_0 = 1$ for incommensurism, $V/V_0 = 0.5$ for coincidence, $V/V_0 = 0$ for commensurism on nonhexagonal substrates, and $V/V_0 = -0.5$ for commensurism on hexagonal substrates. The substrate ($\mathbf{a}_1$ and $\mathbf{a}_2$) and overlayer ($\mathbf{b}_1$ and $\mathbf{b}_2$) lattice vectors for a given azimuthal orientation are related through a transformation matrix **C**, in accordance with the following relationship:

$$\begin{bmatrix}\mathbf{b}_1\\ \mathbf{b}_2\end{bmatrix} = \begin{bmatrix}C_{11} & C_{12}\\ C_{21} & C_{22}\end{bmatrix}\begin{bmatrix}\mathbf{a}_1\\ \mathbf{a}_2\end{bmatrix} \qquad (1)$$

When coincidence occurs, among the transformation matrix elements are at least two integers confined to a single column.

As can be seen in the graphs of Figure 5a and c, there is no azimuthal angle in the range between −90° and +90° which determines any sort of registry ($V/V_0 \leq 0.5$) for the observed orientations of 4T films on KAP(010).

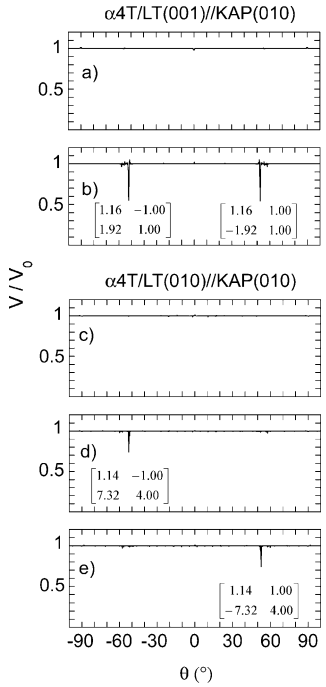

Figure 5. Results of the geometric analysis with EpiCalc of the configurations of the α4T/LT(001) surface (upper panel) and the α4T/LT(010) surface (lower panel) in contact with KAP(010). The azimuthal angle θ corresponds to the angle between a_{4T} and c_{KAP}. Panels a and c represent the curves obtained with the unit cell parameters of the substrate and overlayer, whereas in panels b, d, and e the parameters of the overlayer are doubled. The curves of the two graphs in panels d and e are the results for the α4T/LT(0 1 0) and α4T/LT(0 −1 0) orientations, respectively. The transformation matrixes reported within the graphs refer to the following cell parameters of the substrate and overlayer: $\mathbf{a}_1 = c_{KAP}$, $\mathbf{a}_2 = a_{KAP}$, $\mathbf{b}_1 = 2a_{4T}$, $\mathbf{b}_2 = 2b_{4T}$ for panel b, and $\mathbf{b}_1 = 2a_{4T}$, $\mathbf{b}_2 = 2c_{4T}$ for panels d and e; see eq 1.

To investigate the possibility of "more relaxed" epitaxial relationships, the program allows one to search for "geometric solutions"; i.e., it performs the calculation by using multiples of the unit cell parameters of the overlayer. With this option, coincident orientations are clearly located. For the α4T/LT-(001)//KAP(010) orientation, coincidence is observed when a_{4T} is at ±52° to c_{KAP} (Figure 5b). As far as the α4T/LT(010)// KAP(010) orientation is concerned, due to the monoclinic symmetry of the overlayer, it is worth distinguishing the α4T/LT(010)//KAP(010) orientation from the α4T/LT(0 −1 0)// KAP(010) orientation: in the former, coincidence is observed when a_{4T} is at −53° to c_{KAP} (Figure 5d), whereas in the latter, coincidence is observed when a_{4T} is at +53° to c_{KAP} (Figure 5e). It must be noted that for these *geometric* coincident orientations, a large subgroup of lattice points of the overlayer lies at energetically less favorable positions compared with those that coincide with substrate lattice points.

The experimental texture analysis is presented here by means of pole figures (PFs) collected at the four strongest reflections of the α4T/LT polymorph, i.e., (−113), (−111), (−123), and (021), and reported in Figures 6 and 7.

Figure 6 reports the comparison between series of PFs collected on 4T films deposited on KAP(010) by HWE and MBE. All PFs are characterized by well-defined enhanced pole densities without fiber textures, indicating the high crystallinity and orientational order of the films. The HWE samples show for each pole figure the presence of a crystal orientation contacting the substrate with the (0 0 ±1) planes (squares) and another one with the (0 ±1 0) planes (circles) which, as

(27) (a) Koller, G.; Berkebile, S.; Krenn, J.; Tzvetkov, G.; Hlawacek, G.; Lengyel, O.; Netzer, F. P.; Teichert, C.; Resel, R.; Ramsey, M. G. *Adv. Mater.* **2004**, *16*, 2159. (b) Haber, T.; Oehzelt, M.; Andreev, A.; Thierry, A.; Sitter, H.; Smilgies, D.-M.; Schaffer, B.; Grogger, W.; Resel, R. *J. Nanosci. Nanotechnol.* **2006**, *6*, 698.

(28) Hillier, A. C.; Ward, M. D. *Phys. Rev. B* **1996**, *54*, 14037.

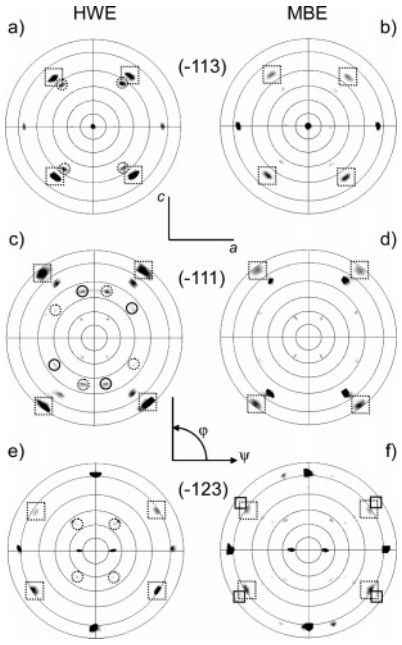

Figure 6. XRD PF measurements of 4T on KAP(010) films grown by HWE and MBE taken from the (−1 1 3) (a,b), (−1 1 1) (c,d), and (−1 2 3) (e,f) reflections of α4T/LT. Each PF is oriented so that the substrate surface *a* and *c* axes are oriented as indicated. Concentric circles are separated by $\Delta\psi = 15°$. Dotted squares indicate reflections coming from the (0 0 1)-oriented film phase, whereas dotted circles indicate reflections coming from the (0 1 0)-oriented film phase. In panel c, reflections belonging to (0 1 0)- and (0 −1 0)-oriented domains are distinguished by dotted and solid circles. Solid squares in panel f indicate reflections coming neither from α4T/LT domains nor from the substrate. All other enhanced pole densities present in the figures are reflections of the substrate.

discussed above, can be related to islands and needles, respectively. The PF reported in Figure 6c is of particular interest, since enhanced pole densities coming from the orientation with (0 1 0) and (0 −1 0) as contact plane can be distinguished (dotted and solid circles, respectively). Comparison with PFs simulated with the structure of the α4T/LT polymorph allowed us to deduce the epitaxial relationship between the needles and the substrate surface lattice. This gives $[1\ 0\ 0]_{4T}||[7\ 0\ 5]_{KAP}$ and $[1\ 0\ 0]_{4T}||[-1\ 0\ 18]_{KAP}$ when $(0\ 1\ 0)_{4T}||(0\ 1\ 0)_{KAP}$, and $[1\ 0\ 0]_{4T}||[-7\ 0\ 5]_{KAP}$ and $[1\ 0\ 0]_{4T}||[1\ 0\ 18]_{KAP}$ when $(0\ -1\ 0)_{4T}||(0\ 1\ 0)_{KAP}$; then, the a_{4T} axis is oriented at ±64.3° and ±4.7° to c_{KAP}. These orientations are very close to those measured in the OM pictures for the needles (±63° and ±5°, with an error of ±2°); this demonstrates that the axes of needles are parallel to a_{4T}. With an analogous procedure, the epitaxial relation for islands gives $[1\ 0\ 0]_{4T}||[0\ 0\ \pm1]_{KAP}$. By observing the difference in intensity between the pole densities marked with dotted squares of the first and second quadrant and the ones of the third and fourth quadrant of the PFs, shown in Figure 6e and f, a slight difference in population of parallel and antiparallel domains with respect to the c_{KAP} axis is deduced. This observation is consistent with previous structural investigations deduced from optical spectroscopy results at oblique incidence[29] and reflects the anisotropic properties of the KAP surface (indeed, the c_{KAP} axis is a polar axis). Since for needles the molecular axes are parallel to the contact plane, we can express the epitaxial relationships referring to the direction connecting the α and ω carbon atoms within one molecule, which is parallel

(29) Tavazzi, S.; Campione, M.; Laicini, M.; Papagni, A.; Sassella, A.; Spearman, P.; Trabattoni, S. *J. Lumin.* **2005**, *112*, 312.

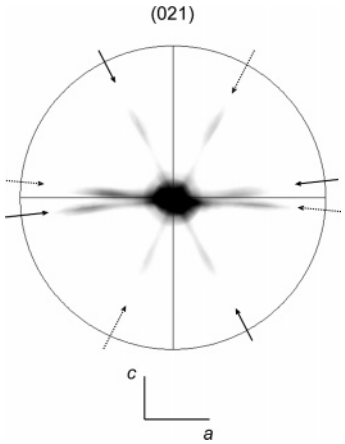

Figure 7. XRD PF measurement of 4T on KAP(010) grown by HWE collected for the (0 2 1) reflection of α4T/LT. The substrate axes are oriented as indicated in the bottom of the panel. The circle is at $\psi = 15°$. Solid and dotted arrows indicate enhanced pole densities of the (0 1 0)- and (0 −1 0)-oriented film phases, respectively.

to $[52\ 0\ 21]_{4T}$. The epitaxial relationships give $[52\ 0\ 21]_{4T}||[5\ 0\ -6]_{KAP}$ and $[52\ 0\ 21]_{4T}||[7\ 0\ 6]_{KAP}$ when $(0\ 1\ 0)_{4T}||(0\ 1\ 0)_{KAP}$, and $[52\ 0\ 21]_{4T}||[-5\ 0\ -6]_{KAP}$ and $[52\ 0\ 21]_{4T}||[-7\ 0\ 6]_{KAP}$ when $(0\ -1\ 0)_{4T}||(0\ 1\ 0)_{KAP}$.

Figure 7 reports a PF of a HWE sample collected at the (021) reflection of 4T, which clearly shows the four orientations of needle-like crystallites; it must be noted that a slight asymmetry characterizes the pole densities corresponding to needle domains at ±4.7° to c_{KAP}. This may be attributed to a contact plane which is slightly tilted with respect to the $(010)_{4T}$ plane, with some component along the c_{4T} direction. Figure 8 depicts schematically the orientation of the molecules and crystal unit cell for the needle-like crystals, as deduced from the epitaxial relationships found above. All four directions of the needle-like crystals observed in the AFM images are comprehensibly explained by an alignment of the molecular axes along the four directions reported above.

The MBE samples give rise to PFs showing only enhanced pole densities corresponding to the phase with $(0\ 0\ \pm1)$ as contact plane, with epitaxial relationships identical to those in the case of HWE samples, i.e., $[1\ 0\ 0]_{4T}||[0\ 0\ \pm1]_{KAP}$. However, four additional weak enhanced pole densities (marked by solid squares in Figure 6f) are present in MBE samples which cannot be assigned to any orientation of a α4T/LT domain. Probably, an unknown polymorph phase of 4T is present in the thin film grown by MBE, which gives rise to diffraction peaks in the specular scan (Figure 4) and in the (−123) pole figure (Figure 6f).[8]

Table 2 summarizes the results of the calculation of the azimuthal orientations predicted with EpiCalc and the orientation observed experimentally with X-ray texture analysis. It is clear that there is no accordance between the two groups of results.

3.3. Potential Energy. We simulated a periodic slab of crystalline KAP with an area of 53.5 × 54.7 Å^2 along the (010) surface exposed to deposition and a thickness of about 27 Å. Its outermost layer consists of aromatic rings, while the first layer of K^+ cations is found about 8 Å below. On this surface, we simulated the deposition of two pre-ordered monolayers of 4T, obtained by "cutting" a thin slab along different planes of the α4T/LT crystal: in one the KAP(010) surface is in contact

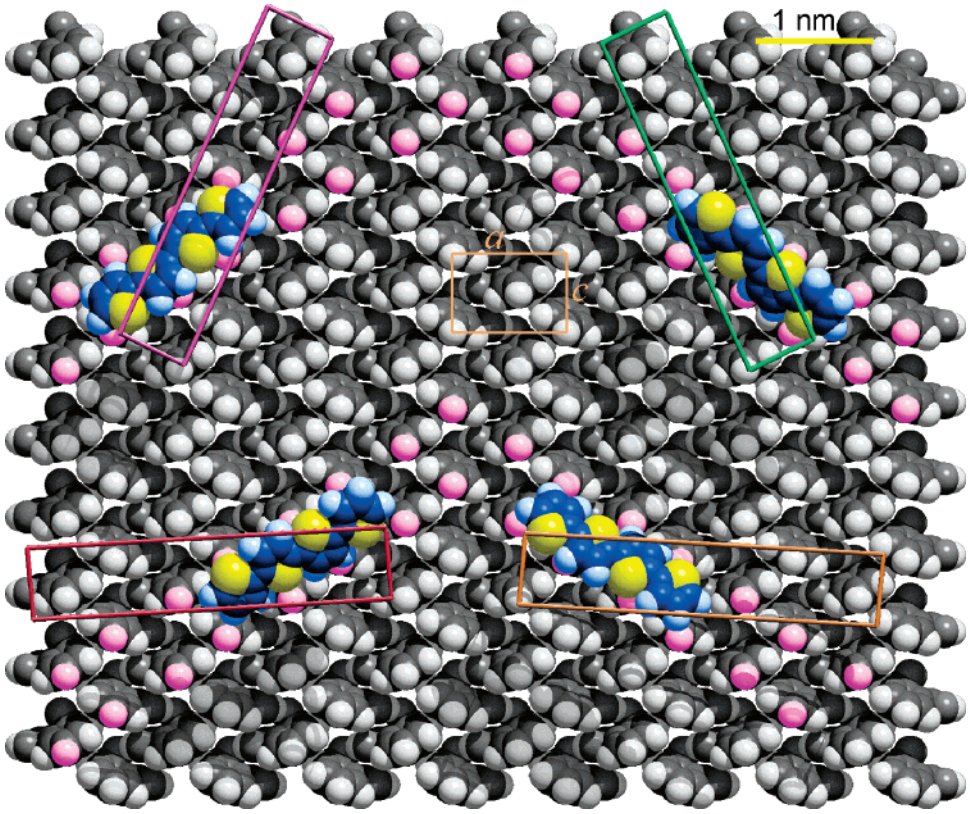

Figure 8. Orientation of 4T molecules and α4T/LT unit cell (*a* short axis, *c* long axis) on KAP(010) for the (0 1 0) (green and red) and (0 −1 0) (purple and orange) phases of 4T, as deduced from the simulations of PFs reported in Figure 6. Prominent H-atoms of the KAP surface are highlighted in purple, and its surface unit cell is depicted in orange.

Table 2. Comparison between Azimuthal Angle (Angle between a_{4T} and c_{KAP}) of the α4T/LT Phase on KAP(010) Predicted with EpiCalc (θ_{calc}) and Observed Experimentally (θ_{exp})

	θ_{calc}	θ_{exp}
4T(0 0 1)	±52°	0−180°
4T(0 1 0)	−53°	−4.7°, +64.3
4T(0 −1 0)	+53°	+4.7°, −64.3°

with the (010) surface of α4T/LT, and in the other it is in contact with the (001) plane of α4T/LT.

We searched for the optimal orientation of each monolayer, changing in 5° steps the angle between c_{KAP} and the average projection on the surface of the long axes of the 4T molecules. Starting from these initial configurations, the energy was minimized with respect to all degrees of freedom. We then plotted the minimized energy values against the final average orientation angle. Typically, this may differ from the starting one by 1−2°. Note that this simple approach produces a set of local minima, which may depend somewhat on the choice of the initial configuration. Despite this shortcoming, our main findings are in good agreement with experiment (see below), and they are also confirmed by a much more extensive simulation study employing a combination of molecular dynamics and energy minimization.[30]

The potential energy profile for the situation when the (010) surface of the α4T/LT crystal is the contact plane with KAP is given in Figure 9. We find that the molecular axes of the 4T molecules have two preferred orientations with respect to

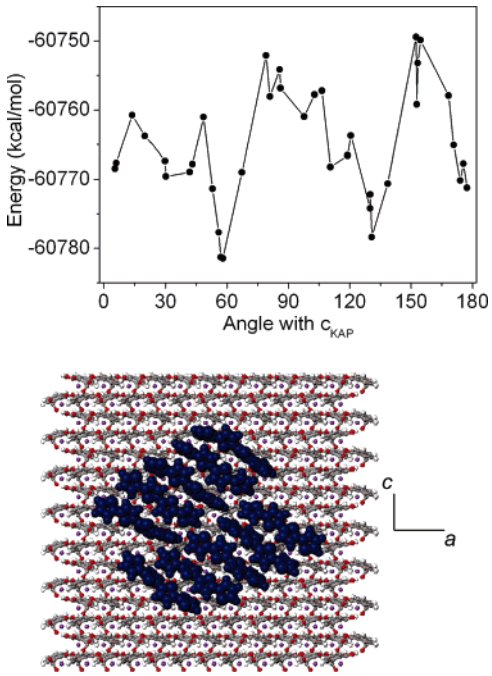

Figure 9. (Above) Potential energy as a function of the orientation of the molecular axes with c_{KAP} of the monolayer of LT crystal exposing the (010) surface on the KAP. (Below) Snapshot of the final configuration of the two minima with the average angle with c_{KAP} = 58°.

c_{KAP}: one with an angle of 58° (this configuration is shown in Figure 9) and the other one with an angle of 131°. The two minima differ in energy by 1 kcal/mol. Note, in the lower part of Figure 9, that the 4T molecules are not fully planar. The

(30) Marcon, V.; Raos, G.; Campione, M.; Sassella, A. *Cryst. Growth Des.* **2006**, *6*, 1826.

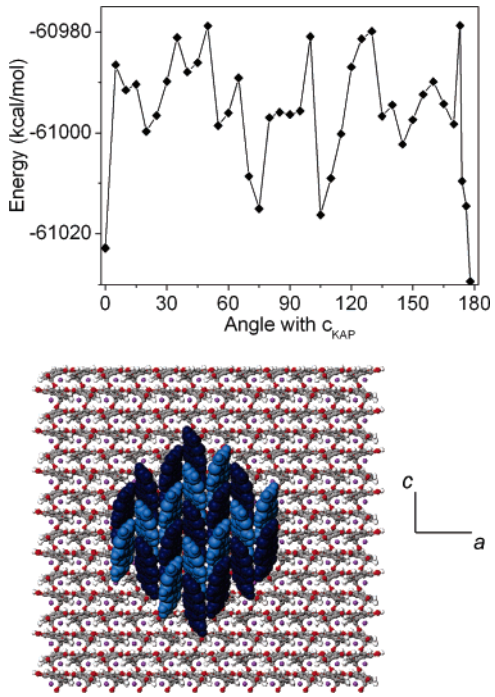

Figure 10. (Above) Potential energy as a function of the orientation of the a_{4T} axis with c_{KAP} of the monolayer of LT crystal exposing the (001) surface on the KAP. (Below) Snapshot of the final configuration of the minima with the angle with $c_{KAP} = 0°$.

asymmetry and jaggedness of the potential energy profile may also be due to this slight conformational disorder.

When the α4T/LT crystal contacts the substrate with the (001) surface, we find two minima at 0° and 180°, where the projection of molecular axes of 4T is parallel to c_{KAP}. There are also two local minima at 73° and 103°. In principle, the first two minima should not be exactly equivalent by symmetry because the c_{KAP} axis is a polar axis. Consistently, their calculated energies differ by a few kilocalories per mole, even if this value is only indicative of the fact that we have not systematically searched for the global minima. The 0° configuration is shown in Figure 10.

For the first case (minimum-energy configuration of the (010) surface of α4T/LT on KAP), we have analyzed the nonbonded contributions to the interaction between one 4T molecule and the substrate. The 4T molecules are located in a groove formed by the hydrogen atoms of KAP, so that they may come into closer contact with the surface. There is also a comparatively large electrostatic interaction between the CH dipoles of the thiophene rings and the oxygen atoms of the carboxylic groups of KAP.

4. Discussion

When considering film nucleation on crystalline surfaces, one of the most important driving forces for the orientation of the overlayer is represented by the lattice match with substrate, namely epitaxy. When organic overlayers are nucleated on organic crystals, the relatively small mismatch between the two lattices may determine a condition of complete incommensurism. As demonstrated in section 3.2, in the case of α4T/LT(001) or α4T/LT(010) on KAP(010), some *geometrical coincidence* characterizes the two lattices. Nevertheless, the in-plane orientations corresponding to these relationships completely disagree with the ones measured experimentally (see Table 2).

Despite the lack of a robust geometrical matching, the results illustrated in the previous sections definitely show that the orientation effect of KAP(010) is very strong and effective, both for islands and for needles. The reason for that rests on the peculiar corrugation of the KAP(010) cleavage surface. This surface is lined with prominent H-atoms of phenyl ring moieties[15] arranged in a herringbone fashion along [001] through H-bonds (see Figure 8). These prominent H atoms (highlighted in Figure 8) form rows along the ⟨101⟩ $_{KAP}$ directions, which form angles of ±55.9° with the c_{KAP} axis and confer a relatively high corrugation to the KAP(010) surface. If we consider the epitaxial relationships found in the HWE samples for the edge-on phase, it is readily noted that the molecules are oriented in such a way that their molecular axis is nearly parallel to the direction of these rows. From this observation, the following mechanism for the nucleation of 4T needles on KAP(010) can be inferred: since the rows of prominent H-atoms are separated by channels with width of the order of the size of a 4T molecule, the diffusion of lying 4T molecules occurs preferably along a direction parallel to the molecular axes, which are in turn parallel to the rows. When the deposited molecules start aggregating to form a crystalline nucleus of α4T/LT, they are already oriented in a way that favors the nucleation of a crystal in which the molecular axes are parallel to ⟨101⟩ $_{KAP}$. This corresponds exactly to a α4T/LT crystal with (0 1 0) or (0 −1 0) as contact plane (see Figure 1) and the azimuthal orientations reported above (i.e., to the 4T needles). Besides this kinetic description of the nucleation of 4T, the results of potential energy calculation (see section 3.3) indicate that the azimuthal orientation found for (010)-oriented 4T aggregates, with all molecules parallel to ⟨101⟩ $_{KAP}$, also corresponds to an energetically favorable situation.

In this scheme, the nucleation probabilities of domains with (0 1 0) or (0 −1 0) as contact plane should be identical; nonetheless, PFs show an intensity slightly higher for enhanced pole densities corresponding to needles oriented at ±4.7° to c_{KAP} (see Figures 6c and 7). This difference in intensity may be related to the misorientation of the contact plane of these needles, as deduced from Figure 7. As far as such a misorientation is concerned, in some AFM images collected on very thin samples (see Figure 11a), needles oriented at ±4.7° to c_{KAP} are sometimes observed to grow across two terraces of KAP separated by an elemental step. This orientation is associated with an apparent high-index contact plane, such as that deduced from the results reported in Figure 7. Since steps present on the KAP(010) surface are preferably oriented along the ⟨101⟩$_{KAP}$ directions[15] (at ±55.9° to c_{KAP}), a similar phenomenon is far less likely for needles oriented at ±64.3° to c_{KAP}. On the contrary, the closeness of these two directions is believed to decrease, to some extent, the energy barrier for the nucleation of needles; for this reason, a high density of needles is frequently observed along ⟨101⟩$_{KAP}$ steps (Figure 11b).

Now we consider the interface between the flat islands and the KAP(010) substrate. Also in this case, substrate and overlayer lattices are incommensurate, so that the orientation of this phase observed experimentally and predicted theoretically (see section 3.2) cannot be directed by lattice match at particular azimuthal orientations. Again, we may ascribe the strong orientation effect of the KAP(010) surface relative to the crystalline 4T islands to the presence of rows of prominent

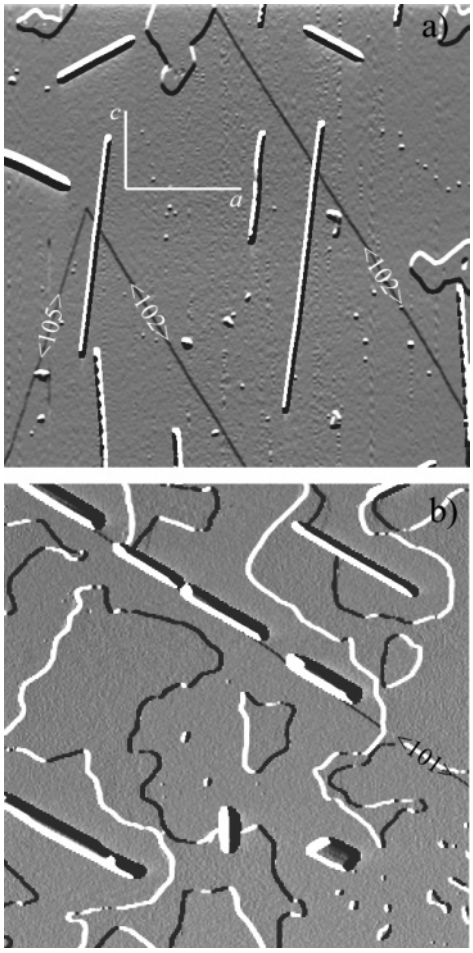

Figure 11. (a) 12 × 12 μm^2 AFM image (error signal) of the surface of a 2 nm thick 4T film grown on KAP(010) by MBE, showing needle-like crystallites between two KAP terraces. (b) 5 × 5 μm^2 AFM image (error signal) of the surface of a 10 nm thick 4T film grown on KAP(010) by MBE, showing needle-like crystallites nucleated along $\langle 101 \rangle_{KAP}$ steps. The orientation of the substrate *a* and *c* axes is reported, together with the crystallographic direction of the steps present on its surface.

H-atoms. Indeed, when the a_{4T} axis is parallel to c_{KAP}, the $[101]_{KAP}$ direction is only 3.8° different from the $[110]_{4T}$ direction. If we consider that the $\langle 110 \rangle_{4T}$ direction corresponds to the direction connecting nearest neighbors within a single α4T/LT layer (see Figure 1c), under the previous epitaxial relationship, compact rows of prominent H-atoms of the thiophene moiety of the $(001)_{4T}$ plane are almost parallel to the grooves defined by the H-atoms of the substrate surface. The match between these directions drives the orientation of the islands. Figure 12 depicts the orientation of the surface lattice of islands relative to the KAP(010) surface, showing the match between the $\langle 101 \rangle_{KAP}$ and the $\langle 110 \rangle_{4T}$ directions.

The diffraction analysis of the MBE films gives no evidence of the presence of an edge-on phase of the α4T/LT polymorph. Nevertheless, we see needles in the AFM images (see Figures 2b, 3, and 10) oriented exactly like the needles present in the HWE films (see Figure 2a), we have additional diffraction peaks in a 2θ range characteristic of interplanar distances of planes parallel to the molecular axes (see Figure 4), and we have additional enhanced pole densities in PFs that cannot be ascribed to the substrate (see Figure 6). These observations can find a possible explanation if we assume that, under the growth

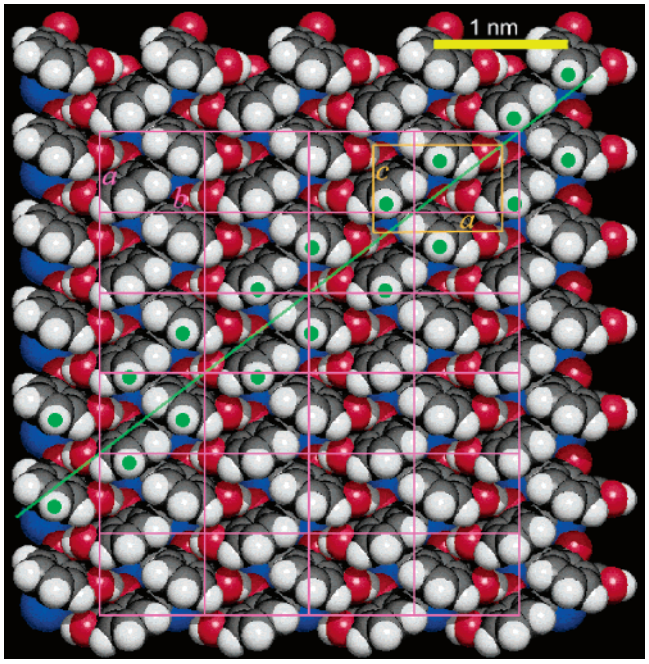

Figure 12. Orientation of the α4T/LT surface lattice (purple) on the KAP-(010) surface for the (001) film phase. The substrate surface unit cell is depicted in yellow. Prominent H-atoms of the KAP(010) surface are highlighted in green. The green line is parallel to the $[110]_{4T}$ direction.

conditions of MBE, needles crystallize in a polymorph different from the known α4T/LT and α4T/HT and not yet identified.

5. Summary and Conclusions

The drive toward all-organic electronics provides a strong technological motivation for improving our understanding of the growth of organic thin films on organic substrates. The optimal performance of electronic devices based on such systems requires the achievement of a high degree of order in the layers over large areas. Generally speaking, the large size and the low symmetry of the unit cells of both substrate and overlayer imply that full or partial registry between their crystal lattices is not so easily achieved, compared to inorganic−inorganic and organic−inorganic systems. We are thus facing two apparently conflicting issues: the requirement for well-ordered films and the difficulty of epitaxy between the substrate and overlayer. Here we described the growth of 4T thin films on the (010) surface of KAP by two sophisticated vapor-phase techniques, namely HWE and MBE. The interface between these materials is characterized by a lattice mismatch as large as 18%. We provided experimental and computational evidence that *molecular epitaxy*, whereby the specificity of the substrate−film interaction depends on molecular-level details in the topography of the crystal surfaces, may produce strong orientation even when there is complete incommensurism between the unit cells. Even if 4T is only one representative material within the vast array of organic semiconductors, we believe that this conclusion might be transferable to other organic molecular materials, opening interesting opportunities for future developments.

We find that the KAP(010) surface is able to totally orient the 4T crystalline domains nucleating on top of it with (001) as contact plane. 4T nuclei with (010) as contact plane are also present on the KAP(010) surface and give rise to needle-like crystallites oriented along particular high-index crystallographic directions of the substrate surface. All the epitaxial relationships

deduced by XRD analysis on this system agree with those predicted theoretically by potential energy calculations and are explained by an alignment of the axes of 4T molecules crystallized in the α4T/LT polymorph along the ⟨101⟩ crystallographic directions of KAP, which correspond to the directions formed by H-atoms protruding from the substrate surface. This demonstrates that the driving force for the orientation of crystalline domains is represented not by a possible lattice match achieved for particular azimuthal orientation of the substrate and overlayer lattices, but rather by the crystallo-chemical properties of the substrate surface, namely its corrugation. The use of the two different growth techniques has highlighted the possibility to tune, to some extent, the film morphology and structure, while epitaxial relationships remain unchanged and are determined by the properties of the substrate surface. In particular, the near-equilibrium conditions of HWE favor the growth of a crystalline bulk-like phase with the structure of the α4T/LT polymorph and molecules lying flat on the substrate. Under the conditions of HWE, nucleation and growth show strongly thermodynamically favored characteristics. In MBE samples, in contrast, the formation of either flat terraces or needles can be enhanced (or limited) by a proper choice of the growth parameters: this can be clearly related to the far-from-equilibrium conditions characteristic of MBE which, in addition, can easily be tuned. Finally, the presence of a small fraction of edge-on crystalline domains of a polymorph different from both α4T/LT and α4T/HT is suggested by XRD data collected on the MBE films. There are indeed other instances, for example in the pharmaceutical context,[7c] where the adoption of vapor-phase deposition on organic substrates has provided a new tool to control crystal growth and discover new polymorphs.

Acknowledgment. The authors thank the Austrian-Italian Academic Exchange Program for support of this work. Thomas Haber and Peter Spearman are kindly acknowledged for fruitful discussions. Malena Oliveros Collantes is also acknowledged for her help in the synthesis and purification of 4T.

JA058771W